AUTHOR and OTHER-AUTHOR

[Left hand page running head is author's name in Times New Roman 8 point bold capitals, centred. For more than two authors, write **AUTHOR et al.**]

CONFERENCE PRE-PRINT

RESEARCH ON NEW HIGH-STRENGTH STRUCTURAL MATERIALS FOR LOW-TEMPERATURE APPLICATIONS IN THE NEXT GENERATION OF FUSION REACTORS

Weijun Wang^{a*}, Yifei Wu^a, Ruzong Zhai^b, Zhengping Tu^c, Xiaogang Shen^c, Huan Jin^a, Jinggang Qin^a

- ^a Hefei Institutes of Physical Science, Chinese Academy of Sciences, Hefei, 230031, PR
- ^b Institute of Metal Research, Chinese Academy of Sciences, Shenyang 110016, PR China
- ^c Zhejiang JiuLi Hi-Tech Metals Company Ltd., Huzhou, Zhejiang 313012, PR China Email: weijun.wang@ipp.ac.cn; qinjg@ipp.ac.cn

Abstract

The jacket layer of superconducting magnets in tokamak fusion reactors must endure extreme electromagnetic-thermal-mechanical loads. Based on Nitronic-50 (N50) austenitic stainless steel, China has developed a modified version of stainless steel, designated as CHSN01 (Cryogenic High-Strength No.1). This study systematically investigates the effects of cold working (CW: 0%, 5%, 10%, 20%) and long-term cryogenic exposure on its mechanical behavior and microstructure. Tensile, fracture toughness, and fatigue tests were conducted at 300 K, 77 K, and 4.2 K, complemented by SEM, EBSD, TEM, and XRD analyses. Results identify an optimal CW deformation (5%), where synergistic strengthening via dislocation networks and deformation twins achieves an optimal strength-ductility balance. Excessive CW induces work hardening saturation and embrittlement, while insufficient CW undermines strengthening. Furthermore, prolonged liquid He exposure did not degrade performance, confirming the viability of CHSN01 for next-generation fusion magnets under extreme operational conditions. This work provides critical data and theoretical support for future optimization of processing techniques for fusion reactor jacket materials.

1. INTRODUCTION

The tokamak is a toroidal magnetic confinement device utilized for nuclear fusion research, employing magnetic fields to contain high-temperature plasma in an effort to achieve clean and sustainable nuclear fusion energy [1]-[3]. As a strategic initiative, China is currently developing the China Fusion Engineering Demo Reactor (CFEDR). This advanced experimental facility aims to address the technical challenges in transitioning from the International Thermonuclear Experimental Reactor (ITER) to a future Fusion Demonstration (DEMO) reactor [4]-[7]. The CFEDR central solenoid (CS) coil is expected to operate at a magnetic field of more than 17 T and a current of 60 kA [8]. The power of nuclear fusion is proportional to the fourth power of the magnetic field intensity. To excite a stronger magnetic field, the CFEDR CS magnet will use a structure of hybrid high and low temperature superconductors (HTS & LTS). Among them, high-performance Nb₃Sn is selected as the lowtemperature superconductor, while REBCO and Bi-2212 are the candidate materials for high-temperature superconductors. The CFEDR CS coil will keep using a Cable-In-Conduit Conductors (CICC) structure. When energized, the jacket layer of superconducting magnets must endure extreme electromagnetic-thermal-mechanical loads, with its performance closely linked to its cold working process and microstructure. According to the current design and operational conditions of CFEDR's CS magnets, future jacket materials must meet the following mechanical property requirements: a yield strength (YS) exceeding 1500 MPa, ultimate tensile strength (UTS) exceeding 1800 MPa, elongation (EL) at break exceeding 25%, and a fracture toughness (K_{IC}) target value of at least 130 MPa·m^{1/2} at 4.2 K ^{[9],[10]}. In addition, it is also required that the jacket materials be non-magnetic. Cryogenic jacket materials such as 316L, 316LN, and JK2LB have been developed for the ITER project. However, these materials exhibit a yield strength of no more than 1100 MPa at 4.2 K, even after cold working (CW) to 20%, making it challenging to meet the required specifications. [11]-[15].

Nitronic-50 (N50), also called UNS S20910 and XM-19, is a non-magnetic, corrosion-resistant, high-strength, weldable (to a certain extent), nitrogen-strengthened austenitic stainless steel. Developed in 1960 by Armco Steel, it is used for manufacturing mechanical parts and equipment with high strength, high precision, and high corrosion resistance, such as in aerospace, petrochemical, automotive manufacturing, and other fields. Japan plans to utilize N50 in the superconducting magnet structural materials and CS tie plates of the JA DEMO. Meanwhile, the Commonwealth Fusion has selected N50 for the structural casings and Nitronic-40 for the radial plates in the Smallest Private-Funded Affordable Robust Compact (SPARC) TF Model Coil application. China has developed a modified version of the traditional N50, which was once named modified N50 and N50H, and

was eventually named Cryogenic High-Strength No.1 (CHSN01), and significantly optimized its low-temperature mechanical properties by completely eliminating δ ferrite and strictly controlling the alloy's carbon (0.01% max) and oxygen (20 ppm max) content, making it a candidate material that meets the requirements. Relevant research work has been conducted on the mechanical properties of CHSN01 jacket material at low temperatures, and the complete preparation process of the jacket has been verified. The YS of CHSN01 jacket material > 1550 MPa, $K_{IC} > 150$ MPa·m¹/² [9],[10].

The CICC conductors must undergo cold working processes, including compression, bending, and straightening during the preparation process. Under different cold working deformations, the microstructure evolution of the CHSN01 jacket and the mechanical performance limits under extreme working conditions are unknown. Therefore, conducting in-depth research on the relationship between the microstructure evolution and mechanical performance will be of great significance for the future application of jacket materials in fusion reactors. Additionally, the deformation mechanism of CHSN01 under strain, as well as the changes in its material properties over long-term exposure to cryogenic temperatures of ~4.2 K, remain unclear. This study accordingly evaluated the mechanical properties and microstructural evolution of CHSN01 conductor jacket material under long-term cryogenic service conditions.

2. EXPERIMENTAL SECTION

2.1. Experimental material and service conditions



Fig. 1 The cold working process of the jacket



Fig. 2 The jacket cross-sectional diagram.

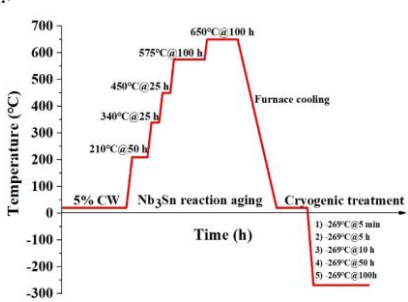


Fig. 3. Curves depicting the 5% CW and Nb₃Sn RA treatments and liquid He exposure durations of the test specimens.



Fig. 4 Tensile specimen. (unit: mm)

AUTHOR and OTHER-AUTHOR

[Left hand page running head is author's name in Times New Roman 8 point bold capitals, centred. For more than two authors, write AUTHOR et al.]

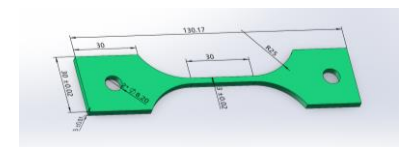


Fig. 5 Fracture toughness CT specimen. (unit: mm)

The CHSN01 CICC jacket sample (Number: 24-342-1-21) with an outer square and inner round shape was provided by the Jiuli Company. An inductively Coupled Plasma Optical Emission Spectrometer (ICP-OES) was used for billet composition analysis, where a Pulse Infrared Thermal Conductivity Analyzer obtained hydrogen and oxygen content.

During CICC coil manufacturing, the jacket needs to be compressed, bent, straightened, wound, and Nb₃Sn superconductor reaction aging treatment. The CHSN01 jacket sample was evenly divided into four parts according to length. As shown in Fig. 1, after undergoing different degrees of CW through the diameter reducing machine, the cold working deformation amounts were calculated by measuring the elongation of the jacket sample in the longitudinal direction, which were 0%, 5%, 10%, and 20% respectively. The cross-sectional diagram of the jacket is shown in Fig. 2. The Nb₃Sn superconductor reaction-aging (RA) treatment follows a specific temperature—time profile comprising the application of 210 °C for 50 h, 340 °C for 25 h, 450 °C for 25 h, 450 °C for 100 h, and 650 °C for 100 h. The detailed preparation procedure for this component can be found in our previous study. Following the CW and RA treatments, the jacket is deployed for long-term service at liquid He temperatures.

The jacket test specimen preparation process is illustrated in Fig. 3. Typical CHSN01 jackets were subjected to CW and RA treatments, then mechanical test specimens were sampled from them using wire electrical discharge machining. Finally, the extracted specimens were immersed in a liquid He dewar during experimentation to simulate the jacket service conditions.

The samples were taken from the C0, C5, C10, and C20 jackets, respectively. Various mechanical property standard samples, including tensile and fracture toughness, were extracted from the four jackets through precise wire-cutting methods. The tensile samples were obtained from the surface of the jackets along the longitudinal direction (LD) by wire cutting, and six tensile samples were taken from each of the four types of jacket, for a total of 24 tensile samples. As shown in Fig. 4, tensile test specimens are prepared in accordance with ASTM E1450. The fracture toughness compacted tension (CT) specimen was taken out along the LD of the jacket sample, with pre-formed crack openings on the specimen. The fracture toughness CT specimens shall conform to JIS Z 2284 standard. As shown in Fig. 5, the fracture toughness CT specimens were prepared: W = 25 mm with a thickness of 2.5 mm without side grooves for the fracture toughness test.

2.2. Experimental method

All mechanical test samples (tensile, fracture toughness, and FCGR) were tested at the Institute of Plasma Physics, Chinese Academy of Sciences. When tested at 4.2 K, the samples are placed in a thermal insulator sleeve and always immersed in liquid helium. All the microscopic analyses of the samples were conducted at the Institute of Metal Research, Chinese Academy of Sciences.

The tensile tests were conducted in a testing machine (Instron 8802). The tensile tests were conducted under displacement control, with the equivalent strain rate: $5 \times 10^{-4}~\text{s}^{-1}$. During the test, the strain was measured using a 10% strain range clamping extensometer (Epsilon model 3542-025M-50-LT). From this, the test results of YS, EL, and UTS at 300 K (RT), 77 K, and 4.2 K were obtained. The fracture toughness tests were carried out in an electro-hydraulic servo testing machine (Instron 8802) at RT, 77 K, and 4.2 K. The CT specimens were pre-cracked at room temperature with a frequency of 3 Hz. The procedure was carried out under constant load control with a stress ratio of R = 0.1. Then, the fracture toughness was measured by the J-integral technique. After the effective elastic-plastic fracture toughness J_{IC} value was measured, the fracture toughness K_{IC} value was converted [10].

To determine the microstructure and distribution of the four jacket samples (C0, C5, C10, and C20), image data were obtained using the Symmetry S2 EBSD probe from Oxford, UK, and data analysis was conducted using AZtecCrystal software. The rectangular samples of $10~\text{mm} \times 10~\text{mm} \times 5~\text{mm}$ were cut on four jackets by wirecutting, and different types of SiC paper for step-by-step mechanical grinding from $150~\text{mm} \times 10~\text{mm}$ to $150~\text{mm} \times 10~\text{mm}$ to $150~\text{mm} \times 10~\text{mm}$ to $150~\text{mm} \times 10~\text{mm}$ and $150~\text{mm} \times 10~\text{mm}$ to $150~\text{mm} \times 10~\text{mm}$

acid and anhydrous ethanol in a volume ratio of 1:9 at room temperature, with a voltage set at 20 V and a duration of 20 seconds. To characterize the fracture morphology and microstructure of CHSN01 stainless steel jacket samples under different CWs deformations, scanning electron microscopy (SEM, Zeiss Sigma 300) and electron back-scattered diffraction (EBSD, Oxford Xplore 30) were used. As shown in Fig. 6, SEM scanning was conducted on the fracture surface of the sample, and EBSD scanning was performed on the diameter reduction and parallel sections to observe the microstructure distribution.

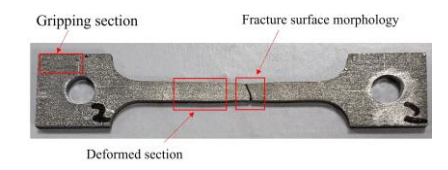


Fig. 6 Microscopic analysis location map of the sample.

3. RESULT

3.1. Tensile test results

The results of YS and EL are shown in Fig. 7 and Fig. 8, respectively. At 300 K, 77 K, and 4.2 K, compared with the samples after CW, the YS of the C0 samples is the lowest and the EL is the highest. The YS of the samples after CW are all greater than the requirement of 1500 MPa at 4.2 K. Moreover, as the cold working deformation increases, the YS shows an upward trend, but the EL shows a downward trend. It is indicated that the CHSN01 stainless steel jacket exhibits obvious work-hardening characteristics. Reasonable CW deformation can significantly enhance its strength, but to some extent, it will sacrifice its plasticity. Notably, it was found that at 300 K and 77 K, EL was highly sensitive to the increase in cold working deformation and would decrease significantly, while at 4.2 K, the downward trend of EL was not obvious. In addition, under the same deformation amount, the elongation of the sample at 77 K is higher. The excellent plasticity of CHSN01 austenitic stainless steel at 77 K may be attributed to the transformation of the deformation mechanism (TRIP/TWIP effect) and the enhanced work hardening ability. At 4.2 K, the C5 specimens achieved the optimal balance between strength and ductility (YS > 1500 MPa; elongation > 30%).

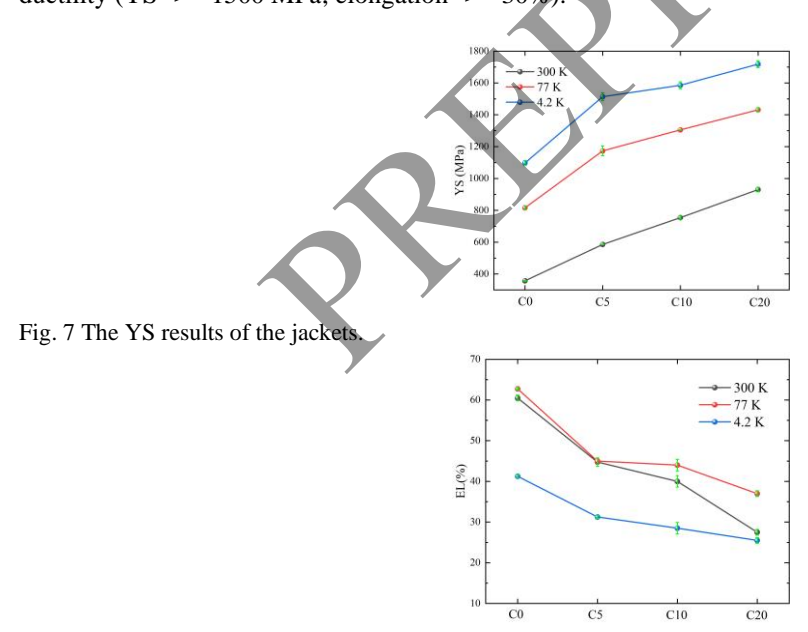


Fig. 8 The EL results of the jackets.

3.2. K_{IC} test results

Fig. 9(a) shows the variation curves of load with crack propagation and diffusion displacement recorded in the experimental tests of the CHSN01 jacket under four CW deformation amounts. As the CW deformation increases, the integral area under the curve gradually decreases, indicating that the toughness of the jacket sample deteriorates. The J_{IC} curve at 4.2 K is shown in Fig. 9(b), and converted to K_{IC} according to the standard of JIS Z 2284. Fracture toughness K_{IC} test results are shown in Fig. 10. At 300 K, 77 K, and 4.2 K, CW

[Left hand page running head is author's name in Times New Roman 8 point bold capitals, centred. For more than two authors, write

AUTHOR et al.]

has a certain impact on fracture toughness. The Fracture toughness of the jacket decreases with the increase of cold working deformation, and the toughness deteriorates. At 4.2 K, the average K_{IC} of C0, C5, C10, and C20 are 264 MPa·m^{1/2}, 249 MPa·m^{1/2}, 225 MPa·m^{1/2}, and 213 MPa·m^{1/2}, respectively, and the decrease was smaller than that at 77 K and 300 K. In future CHSN01 jacket applications, although adding CW deformation can enhance the strength to a certain extent, its toughness is also decreasing.

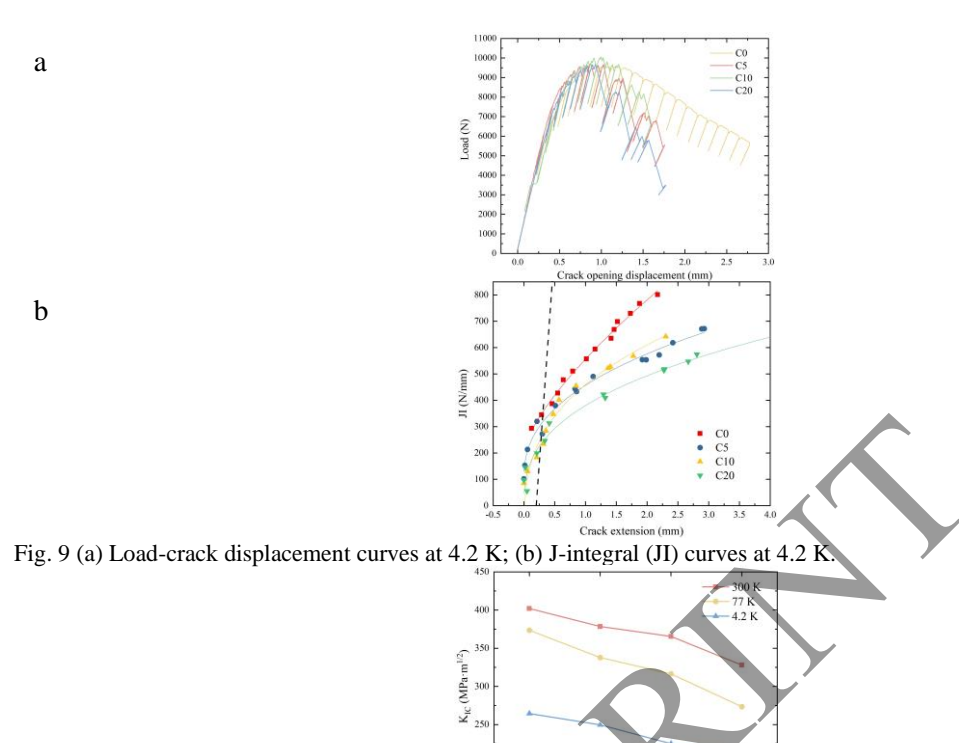


Fig. 10 Fracture toughness K_{IC} test results of the samples.

3.3. Mechanical test results of different liquid He exposure durations (5% CW and Nb₃Sn RA treatments)

Table 1. Average mechanical test results obtained at 4.2 K.

Soaking time	YS (MPa)	UTS (MPa)	EL (%)	K _{IC} (MPa·m ^{1/2})
5 min	1587	1833	32.5	190
5 h	1562	1831	34	212
10 h	1555	1832	35.8	188
50 h	1566	1835	30.1	199
100 h	1562	1846	34.6	185

The mechanical properties of the test specimens immersed in liquid He for different durations were evaluated through tension and fracture toughness testing at 4.2 K to obtain their average YS, UTS, EL, and KIC values. The results are listed in Table 1.

4. DISCUSSION

4.1. Tensile fracture analysis

The SEM images of the CHSN01 jacket samples with four deformation amounts are shown in Fig. 11. The ductile fracture characteristics are presented in all four states. Four samples exhibited microvoid coalescence fracture dominated by dimple structures. The C0 sample showed typical ductile fracture, with uniform distribution of relatively large equiaxed dimples. It indicates that the jacket has excellent plasticity in this state, which is consistent with the mechanical performance of high elongation.

The number of dimples in C5 has increased while their size has decreased. Some dimples exhibit an elongated tendency due to slight grain deformation. CW deformation increases dislocation density, and the slip zone leads to local stress concentration, thereby enhancing the strength of the jacket while reducing its plasticity.

The fracture characteristics reflect the initial equilibrium shift between strength and ductility. The dimples of C10 have been significantly refined, with a sharp increase in their number. The increase in deformation leads to the extensive diffusion and entanglement of dislocations and severe elongation of grains, resulting in a continuous increase in strength and a continued decrease in elongation. Notably, the C20 macrofractograph displayed extensive secondary cracks and shear lips, likely attributed to high dislocation density introduced by 20% room-temperature pre-deformation, which induced significant internal stress concentration and increased intergranular misorientation. During deformation at 4.2 K, cracks propagated preferentially along low-energy dissipation paths (some specific slip systems), while encountering high-angle grain boundaries caused abrupt crack path deflection. This phenomenon generated numerous shear lips and secondary cracks, reflecting substantial plasticity loss. The excessive plastic deformation loss directly correlates with the drastic reduction in elongation observed in 4.2 K tensile tests.

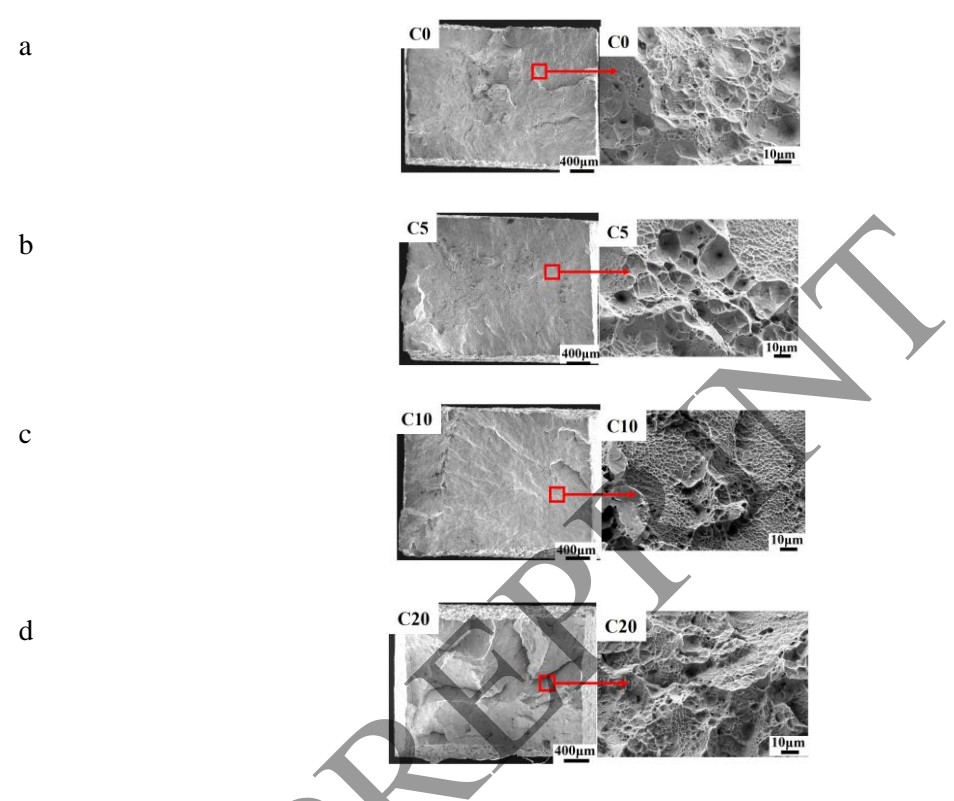


Fig. 11 SEM figures of CHSN01 jacket. ((a): C0; (b): C5; (c): C10; (d): C20)

4.2. EBSD analysis

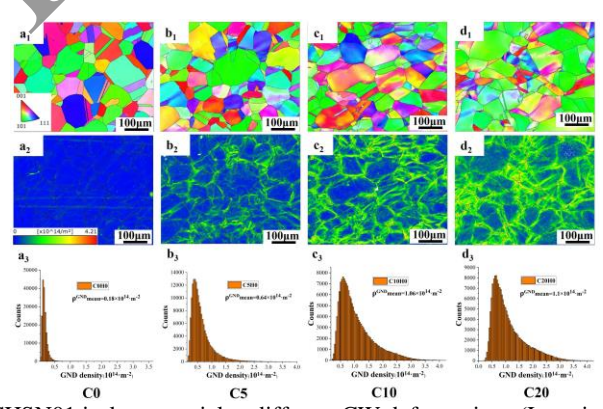


Fig. 12 The EBSD images of CHSN01 jacket material at different CW deformations (Location: gripping section): (a1-d1) Inverse pole figures, (a2-d2) GND distribution image, (a3-d3) GND statistics.

The gripping section of the tensile sample did not undergo deformation during the tensile test at 4.2 K. Fig. 12 demonstrates that in the undeformed state, the grains exhibit equiaxed morphology with some annealing twins. In the C0 state, the grains exhibit an equiaxed morphology with a relatively uniform size distribution. The C5 specimen shows localized color banding and an increased proportion of low-angle grain boundaries (LAGBs).

AUTHOR and OTHER-AUTHOR

[Left hand page running head is author's name in Times New Roman 8 point bold capitals, centred. For more than two authors, write **AUTHOR et al.**]

Dislocation motion initiates, leading to dislocation pile-ups at grain boundaries and the development of some subgrain boundaries. The C10 specimen exhibits extensive dislocation multiplication and progressive refinement of substructure. The C20 specimen exhibits some grain fragmentation, accompanied by loss of coordinated deformation capacity, continued sub-grain boundary proliferation, and approaching saturation of work hardening. Among them, no strong texture is developed, as evidenced by the mixed distribution of primary colors, though the local orientation gradient increases. The pre-deformation does not cause an obvious orientation priority phenomenon.

With the increase of pre-deformation, it can be seen from Fig. 12(a2-d2) that the dislocation density increases gradually. In the statistical distribution of Geometrically Necessary Dislocation (GND) densities, the counting peak predominantly concentrates within the low-density region, as shown in Fig. 12(a3-d3). The GND density refers to the total length of the dislocation line in a unit volume of crystal. With the increase of predeformation, dislocation strengthening takes the lead: the GND of C0 rises from 0.18×10^{14} m⁻² to 1.1×10^{14} m⁻², which has increased by 255%, indicating that the initial deformation triggered substantial dislocation multiplication, directly enhancing the strength. This phenomenon perfectly matches the well-known statistical dislocation model - the Taylor reinforcement formula:

$$\Delta \sigma = \alpha M \mu b \sqrt{\rho} \tag{1}$$

Among them, α is the strengthening constant (\sim 0.3), M is the Taylor factor, μ is the shear modulus, b is the Burgers vector, and ρ is the dislocation density. For specimen C5, the theoretical strength increase of about 160 MPa aligns well with the experimentally measured increment of 155 MPa. The greater the deformation, the denser the dislocations, and the more difficult it is for the material to undergo plastic deformation. When the deformation reaches 20%, the density growth of GND slows down, and further increasing the amount of CW deformation may lead to embrittlement, causing the jacket to crack. The mechanical properties show a pattern of "increased strength and decreased elongation", which is essentially the result of the effect of work hardening.

Conclusion

This study systematically evaluates the comprehensive performance of the domestically developed CHSN01 high-strength and high-toughness stainless steel conductor jacket under extreme service conditions in fusion devices. The results demonstrate that the CHSN01 jacket exhibits a YS exceeding 1500 MPa at 4.2 K while maintaining excellent ductility (EL > 30%), meeting the requirements for engineering applications and achieving mass production. Experiments involving different pre-deformation levels and prolonged liquid helium exposure revealed that the mechanical behavior is primarily governed by work hardening, with an optimal strength—ductility balance achieved at 5% cold working (CW). Furthermore, the material displayed exceptional structural stability under extended cryogenic conditions, showing no phase transformation or degradation in mechanical properties, which confirms its capability for long-term service in liquid helium environments. Batch production of CHSN01 jackets capable of withstanding 650 °C Nb3Sn heat treatment without embrittlement has been successfully realized in China. This study provides important theoretical and experimental support for optimizing the processing technology and achieving a better balance between strength and ductility in fusion reactor jacket materials.

REFERENCES

- [1] Ding, S., Garofalo, A. M., Wang, H. Q., et al. A high-density and high-confinement tokamak plasma regime for fusion energy. Nature, 2024, 629: 555–560.
- [2] Dimits, A. M., Bateman, G., Beer, M. A., et al. Comparisons and physics basis of tokamak transport models and turbulence simulations. Physics of Plasmas, 2000, 7(3): 969 983.
- [3] De Tommasi, G., Albanese, R., Ambrosino, G., et al. Current, position, and shape control in tokamaks. Fusion Science and Technology, 2011, 59(3): 486 498.
- [4] Song, Y. T., Wu, S. T., Li, J. G., et al. Concept Design of CFETR Tokamak Machine. IEEE Trans. Plasma Sci., 2014, 42(2): 503 509.
- [5] Song, Y. T., Li, J. G., Wan, Y. X., et al. Engineering design of the CFETR machine. Fusion Eng. Des., 2022, 183: 113247.
- [6] Wan, Y. X., Li, J. G., Liu, Y., et al. Overview of the present progress and activities on the CFETR. Nucl Fusion, 2017, 57(10): 102009.
- [7] Zhuang, G., Li, G. Q., Li, J., et al. Progress of the CFETR design. Nucl. Fusion, 2019, 59(11): 112010.
- [8] Yin, D., Wu, Y., Han, H., et al. Conceptual Design of CFETR CS Model Coil Structure. IEEE Transactions on Plasma Science, 2018, 46(5): 1507 1511.
- [9] Wang, W. J., Zhao, C. Y., Jin, H., et al. Mechanical Properties Evaluation of ReBCO CICC Jacket Based on Super Austenitic Stainless Steel for CFETR High field Magnet. Nucl. Mater. Energy, 2022, 34: 101344.
- [10] Wang, W. J., Zhao, C. Y., Jin, H., et al. The research on high-strength CICC jackets with YS > 1500 MPa at 4.2 K for future fusion applications. Nucl. Mater. Energy, 2023, 36: 101474.

- [11] Sgobba, S., Libeyre, P., Marcinek, D. J., et al. A comparative assessment of metallurgical and mechanical properties of two austenitic stainless steels for the conductor jacket of the ITER Central Solenoid. Fusion Eng. Des., 2013, 88(11-12): 2484 2487.
- [12] Morra, M. M., Ballinger, R. G., Hwang, I. S., et al. Incoloy 908, a low coefficient of expansion alloy for high strength cryogenic applications: Part I. Physical metallurgy. Metallurgical Transactions A, 1992, 23(12): 3177–3192.
- [13] Hamada, K., Nakajima, H., Kawano, K., et al. Optimization of JK2LB chemical composition for ITER Central Solenoid conduit material. Cryogenics, 2007, 47(3): 174 182.
- [14] Maribel, L., Saucedo Muñoz, Shi, C., Liu, et al. Correlationship between JIC and equivalent fracture strain determined by small punch tests in JN1, JJ1 and JK2 austenitic stainless steels. Cryogenics, 2001, 41(10): 713–719.
- [15] Hamada, K., Nakajima, H., Kawano, K., et al. Demonstration of full scale JJ1 and 316LN fabrication for ITER TF coil structure. Fusion Eng. Des., 2007, 82(11-12): 1481–1486.

